Received: 15 October 2022 | Revised: 4 December 2022 | Accepted: 8 December 2022

DOI: 10.1002/smm2.1178

RESEARCH ARTICLE

SmartMat Open Access WILEY

Highly conductive fiber with design of dual conductive Ag/CB layers for ultrasensitive and wide-range strain sensing

Ben Niu | **Su Yang** | **Yiyi Yang** | **Tao Hua**

School of Fashion & Textiles, The Hong Kong Polytechnic University, Hong Kong SAR, China

Correspondence
Tao Hua, School of Fashion & Textiles, The Hong Kong Polytechnic University, Hung Hom, Hong Kong SAR 999077, China.
Email: tao.hua@polyu.edu.hk

Funding information
Research Grant Council of Hong Kong, Grant/Award Number: 15209420

Abstract

Recently the ever-increasing demand for wearable electronics has greatly triggered the development of flexible strain sensors. However, it is still challenging to simultaneously achieve high sensitivity, wide working range, and good wearability. Herein, we developed a highly stretchable fiber strain sensor based on wet-spun porous polyurethane (PU) fiber, and especially a unique conductive network of dual silver (Ag)/carbon black (CB) layers is constructed. Under strain, the rapid crack propagation on the brittle Ag layer brings a large resistance change and thus high sensitivity, while the tunneling-effect dominated CB layer bridges the separated Ag islands to maintain the integrity of conductive pathways under large strain. By means of the synergistic effect of Ag/CB layers, this composite fiber of Ag/CB@PU presents not only high conductivity of 5139.9 S/m, but also ultrahigh sensitivity with a gauge factor of 2.52×10^6 and a wide working range of up to 200%. Besides that, it is also capable of detecting very tiny strain of 0.1% and working stably for over 8000 cycles. Using mature weaving technology, this fiber strain sensor can be seamlessly integrated into the textile to conformally track different movements of the human body. Together with the facile all-solution-based fabrication protocol, this work proposed a new strategy to prepare high-performance fiber strain sensor, promising the textile-based wearable applications.

KEYWORDS

carbon black, conductive fiber, strain sensor, textile

1 | INTRODUCTION

Promising as an indispensable component of next-generation electronics, wearable and flexible strain sensors are receiving widespread attention on account of their great potentials in applications like personal health monitoring, soft robotics, virtual reality, and so forth.[1–5] Among various performance requirements, comfortable wearability is believed to be one of the important factors for strain sensors in practical

This is an open access article under the terms of the Creative Commons Attribution License, which permits use, distribution and reproduction in any medium, provided the original work is properly cited.
© 2023 The Authors. *SmartMat* published by Tianjin University and John Wiley & Sons Australia, Ltd.

applications. In this regard, the daily textile, a hierarchical fiber assembly worn on the human body, is considered as an ideal platform to accomplish a wearable strain sensing system.[6–8] To grant textile the sensing function, multitudinous approaches have been proposed and two main methodologies have been established.[9–11] The first one is to directly coat conductive materials onto textile substrates through dip-coating,[12–14] vacuum filtration,[15] spray coating,[16] and so forth. Although simple to operate, this method still faces challenges like degraded aesthetic appearance and feeling of textile, poor sensing performance such as low sensitivity, and severe hysteresis mainly arising from the complicated transformation of textile geometry under strain.[10,13,17,18] Alternatively, it is preferable to develop one-dimensional (1D) flexible sensor in a fiber-type configuration for the textile-based wearable system, which can be easily woven or knitted into textile structures with unnoticeable size in wearing, well keeping the inherent merits of textile.[19–23] In addition, the 1D sensor is also advantageous in low-cost and continuous production, simple deformation model under strain, and easily tailorable performance.

Over the past decade, a wide variety of approaches have been put forward to develop 1D fiber-based strain sensors, which can be mainly classified into two types: pure fibers of conductive material like graphene/carbon nanotubes (CNT) fiber,[24,25] and composite fibers combining soft polymers with conductive materials.[22,26–28] In contrast, the composite fibers have much higher stretchability and sensitivity, making them more suitable for detecting human motions with deformation as large as >50%.[10,29] Generally, most of the composite fibers can be prepared via either a coating or blending method to combine conductive materials with an elastic fiber host.[23,30–33] The conductive materials commonly include carbon-based materials, metal nanowires/nanoparticles, and newly emerging liquid metal with both high conductivity and stretchability.[34–36] According to the fabrication strategies and materials used, the conductive composite fibers were reported with different sensing performance in terms of sensitivity, stretchability, stability, and so forth. Despite the significant advances of pioneering research, it still remains challenging to well achieve both high sensitivity and wide sensing range, so that the full-range deformation of human body can be accurately detected. For example, it was reported that a graphite/silk fiber sensor could be easily fabricated by rod-coating.[37] The sensor exhibited a gauge factor (GF) of 14.5 and limited workable strain range of 15%, making it incapable of detecting large strain. Huang et al.[38] utilized polymer nanoball decorated graphene to prepare a porous fiber sensor by wet-spinning, in which the rolling friction of nanoball greatly increased the GF from 5 to 87 within small strain of 8%. Although many other fiber sensors were reported with large workable strain (≥50%), their sensitivities were relatively low (GF < 10), such as the graphene/polyester/polyurethane (PU) fiber (GF of 3.7 within 50%),[39] liquid metal/PU fiber (GF of 1.5 within 500%),[36] CNT/PU yarn (GF of 1.24 within 100%),[22] PU/cotton/CNT core-spun yarn (GF of 0.65 within 300%).[40] Therefore, it is necessary and desirable to explore an efficient method for the fabrication of highly stretchable and sensitive fiber strain sensor.

In this study, we developed a facile strategy to fabricate stretchable and conductive fiber strain sensor based on an elastic and porous PU fiber, which was prepared by scalable wet spinning technology. To grant the PU fiber excellent sensing performance, including both high sensitivity and wide working range, we constructed a conductive architecture including dual silver (Ag) and carbon black (CB) layers. Especially, under strain, the crack-based Ag layer provides a small initial resistance and high sensitivity, while the CB layer can assure the integrity of conductive path under large strain by the tunneling effect. For the preparation process, the widely used CB with good electrical conductivity was firstly adopted to decorate the PU fiber by efficient ultrasonication, and then Ag nanoparticles with superior conductivity was deposited with the aid of polydopamine (PDA). Besides high flexibility and conductivity, the developed 1D fiber sensor also displays prominent sensing performance in terms of ultrahigh sensitivity (GF of 2.52×10^6), wide workable range (200%), fast response (62 ms), and notable durability (8000 cycles). Eventually, a wearable sensing textile was fabricated by directly weaving the as-prepared 1D fiber sensor into specially designed textile structure, which well demonstrates the comfortable and wearable applications of detecting various human motions and physiological conditions.

2 | EXPERIMENTAL SECTION

2.1 | Materials

Thermoplastic PU of Elastollan 1185 A was provided by BASF. CB of Vulcan XC72 was obtained from Cabot. Chemicals of dimethylformamide (DMF), ammonium hydroxide ($NH_3 \cdot H_2O$), hydrochloric acid (HCl), sodium lauryl sulfate (SLS), and tris(hydroxymethyl) aminomethane (Tris) were purchased from Alfa Aesar. Silver nitrate ($AgNO_3$), dopamine hydrochloride, and glucose were bought from Acros, Sigma-Aldrich, and Aladdin, respectively. All of the materials were directly used without further purification.

26888193x, 2023, 6, Downloaded from https://onlinelibrary.wiley.com/doi/10.1002/smm2.1178 by Hong Kong Poly University, Wiley Online Library on [11/04/2024]. See the Terms and Conditions (https://onlinelibrary.wiley.com/terms-and-conditions) on Wiley Online Library for rules of use; OA articles are governed by the applicable Creative Commons License

2.2 | Preparation

Fabrication procedure of the Ag/CB@PU fiber strain sensor mainly involves four steps. First, to prepare the PU fiber by wet-spinning, PU pellets were gradually added and dissolved into the DMF solution under magnetic stirring at 80 °C, with the weight percentage of PU controlled as 20 wt%, and then the PU/DMF solution was injected at a rate of 0.6 mL/min into the coagulation bath of deionized water via a needle with 1.36 mm inner diameter. After complete flocculation in water for 30 min, the PU fiber was dried in air at room temperature. Second, the wet-spun PU fiber was immersed into the CB dispersion (2 mg/mL) and decorated with CB under probe ultrasonication of 450 W for 60 min in ice-water bath. The CB dispersion was prepared by dispersing the CB powders with SLS (1 mg/mL) as surfactant in deionized water under ultrasonication of 450 W for 20 min. Third, after cleaning by deionized water, PDA was applied to modify the fiber surface by dipping into the dopamine hydrochloride solution (2 mg/mL) for 3 h, which was buffered to a pH of 8.5 by Tris-HCl. At last, for the deposition of Ag layer, the PDA-modified fiber was immersed into the Tollens' solution, which was prepared in advance via the addition of diluted NaOH (5 wt%) and $NH_3{\cdot}H_2O$ (2 wt%) into $AgNO_3$ solution (0.1 mol/L),[41] and after plating of 5 min with the addition of glucose (0.2 mol/L) as reducing agent, the final composite fiber of Ag/CB@PU was cleaned by deionized water and dried in oven at 60 °C before further testing. For comparison, the fiber of Ag@PU was prepared by depositing Ag onto PDA-modified PU fiber, where the experimental conditions of PDA modification and Ag deposition keep same with those of Ag/CB@PU fiber.

2.3 | Characterization

The fiber morphologies were observed by a scanning electron microscope (SEM, VEGA3; Tescan), meanwhile with elements mapping analyzed by energy-dispersive X-ray spectroscopy (EDS). Optical images of different fibers were obtained by microscope of Leica M165C. Thermogravimetric analysis (TGA, Mettler Toledo DSC/TGA1) was employed to examine the samples' thermal properties by heating from 50 °C to 600 °C at a heating rate of 20 °C/min under the N_2 atmosphere. The chemical composition of the fiber with different coatings was detected by X-ray photoelectron spectroscopy (XPS, Nexsa G2; Thermo Scientific). The fiber tensile properties were measured by an Instron universal test instrument (model 5566; Instron), with the testing speed of 300 mm/min and gauge length of 20 mm. Sheet resistance of the fiber with different coatings was tested using a four-point probe resistivity meter (HPS2661; HELPASS). As for the strain sensing performance, the fibers with a testing length of 20 mm, were connected with copper wires and firstly prestretched to 200% for one stretching-releasing cycle. Then the fiber sensor was tested by applying different tensile strains by Instron 5566, and simultaneously the resistance change was in-situ recorded by a multimeter of Keithley 2000.

3 | RESULTS AND DISCUSSION

The process for fabricating the Ag/CB@PU composite fiber is illustrated in Figure 1A. First, the cost-effective wet-spinning method was applied to continuously prepare the elastic PU fiber with a diameter of ca. 0.95 mm (Figure 1B). From the tensile stress-strain curve in Supporting Information: Figure S1, the wet-spun PU fiber displays an outstanding flexibility including low Young's modulus of 2.9 MPa and large elongation at break of 410%, making it sensitive to external small stress and sustainable to large strain. Subsequently, to endow the PU fiber conductivity, CB nanoparticles were decorated on the fiber surface by efficient ultrasonication method.[42–44] Under ultrasonication, numerous cavitation bubbles will be generated, and then collapse when approaching the CB nanoparticles. As a result, jets and shock waves with high speed and energy are generated, which enables the intensive hitting of the fast-moving CB nanoparticles toward the fiber surface. Thus, the PU surface becomes softened or even partially melted at the impact sites, finally leading to the firm anchoring of CB nanoparticles onto the fiber surface. As shown in Figure 1B, the black color of CB@PU fiber indicates the successful deposition of CB. Additionally, it is noteworthy that there are two reasons for the selection of CB instead of other carbon materials. On one hand, as a widely applied carbon material, CB is low-cost and commercially available, which benefits the large-scalable fabrication of strain sensors. On the other hand, compared with 1D CNT and 2D graphene,[45,46] the 0D CB owns a much smaller aspect ratio and the interaction between CB nanoparticles is relatively weak. Therefore, the conductive network based on CB is easily destroyed under strain, thus showing a higher sensitivity. Moreover, metallic Ag with high conductivity was deposited by electroless plating. Specifically, to facilitate the Ag deposition onto the CB layer, the fiber surface of CB@PU was modified by PDA to improve the surface wettability. Well known as the mussel-inspired biomacromolecule, PDA is rich in catechol and amine groups, and able to

26888193x, 2023, 6, Downloaded from https://onlinelibrary.wiley.com/doi/10.1002/smm2.1178 by Hong Kong Poly University, Wiley Online Library on [11/04/2024]. See the Terms and Conditions (https://onlinelibrary.wiley.com/terms-and-conditions) on Wiley Online Library for rules of use; OA articles are governed by the applicable Creative Commons License

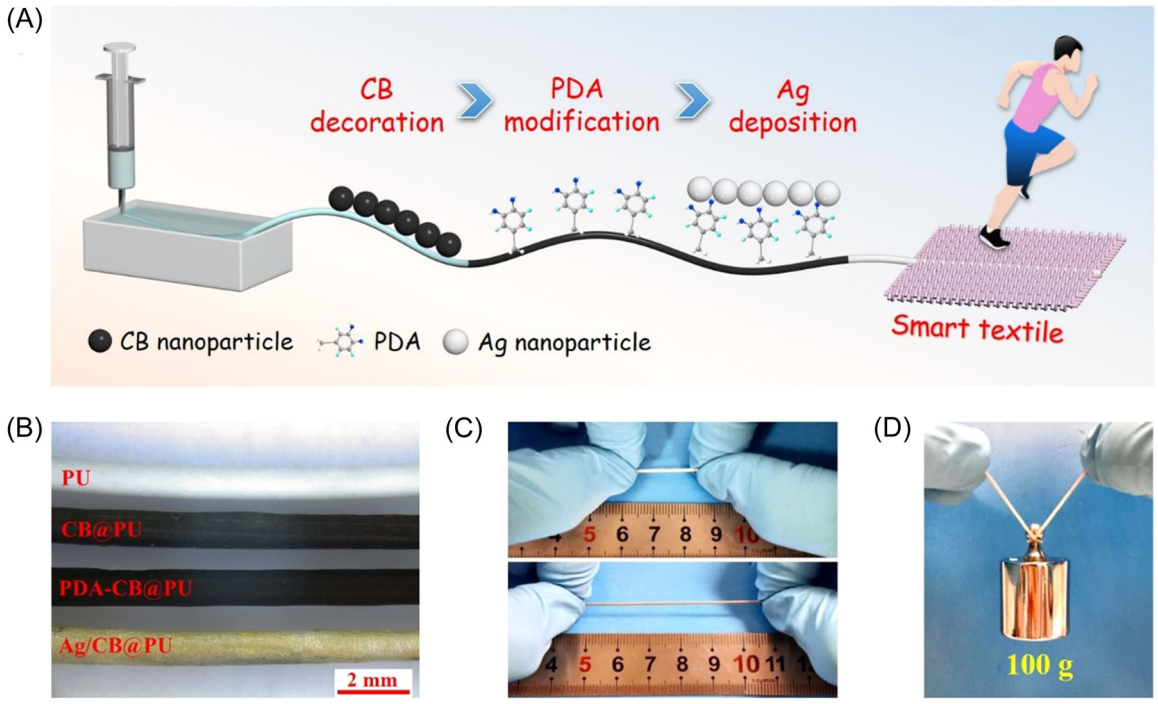

FIGURE 1 (A) Scheme illustrating the fabrication process for the conductive and stretchable composite fiber of Ag/CB@PU. (B) Optical microscope image of different composite fibers, showing the color change of the fiber during the fabrication procedures. (C) Photographs of the pristine and stretched Ag/CB@PU composite fiber. (D) Photograph of a 100 g weight lifted by the Ag/CB@PU composite fiber. CB, carbon black; PDA, polydopamine; PU, polyurethane.

form strong adhesion with nearly all materials' surface by covalent and noncovalent binding.[47] Additionally, the nano-scale thin PDA film can also serve as a secondary reaction platform to reduce metal ions and anchor the resultant metal nanoparticles via coordination and chelating bonding interactions.[47–50] Therefore, PDA modification is believed to be a facile and effective method for the Ag deposition onto CB layer. In detail, the CB@PU fiber was dipped into the dopamine solution, where the dopamine molecules are oxidized and self-assembled into macromolecules of PDA (Supporting Information: Figure S2). Then, after immersing in Tollens' solution, the catechol groups in PDA can chelate with the silver precursor of $[Ag(NH_3)_2]^+$ ions, and reduce the $[Ag(NH_3)_2]^+$ ions into metallic Ag. These Ag nanoparticles can act as crystal nucleus to promote the further growth of Ag layer during the electroless plating process after the addition of a reduction agent (glucose). In addition to the reducibility, the PDA layer is proven to have strong adhesion with the generated Ag nanoparticles via chelating and coordination bonding interactions,[48,50] thus contributing to a stable linking between the Ag and CB layers. As displayed in Figure 1B, the fiber's color obviously changes from black to bright silver, suggesting the formation of Ag layer. In clear contrast, without PDA (Supporting Information: Figure S3), the deposition of Ag on CB@PU surface is difficult and the fiber still stays black after Ag plating. Importantly, compared with other methods like sputtering,[51] atomic layer deposition,[52] and multicycles' dip-coating,[39] the surface deposition methods used herein, that is, ultrasonication and PDA-assisted electroless plating, are time-saving, cost-effective, and easy to operate, which readily prefers scalable and low-cost fabrication. Moreover, the mechanical properties of the PU, CB@PU, and Ag/CB@PU fibers were measured and compared in Supporting Information: Figure S1. In contrast with PU fiber, the coating of relatively hard CB and Ag layers increases the fiber's modulus to 3.8 MPa and 4.0 MPa, and meanwhile with the elongation at break reduced to 365% and 360%. Similarly, during bending, the load value of CB@PU and Ag/CB@PU fibers are higher than that of PU fiber. These results both indicate that the coating of CB and Ag layers can partly increase the fiber rigidity, but it is believed that the Ag/CB@PU composite fiber is still flexible and stretchable enough to sustain a large strain (>300%). From Figure 1C,D, we can see that the obtained Ag/CB@PU composite fiber is highly stretchable and robust to lift a large weight of 100 g. As schemed in Figure 1A, by means of facile fabrication and outstanding stretchability, this composite fiber presents huge potential to be integrated into textile for smart wearable applications.

26888193x, 2023, 6, Downloaded from https://onlinelibrary.wiley.com/doi/10.1002/smm2.1178 by Hong Kong Poly University, Wiley Online Library on [11/04/2024]. See the Terms and Conditions (https://onlinelibrary.wiley.com/terms-and-conditions) on Wiley Online Library for rules of use; OA articles are governed by the applicable Creative Commons License

The morphological development of the composite fibers during fabrication can be directly observed by SEM. As shown in Figure 2A,B, the wet-spun PU fiber presents a porous structure, and there exist a great deal of small pores inside the fiber core with an average diameter of 1.8 μm (Figure 2C). The formation of the porous structure is ascribed to exchange between DMF and water in the coagulation bath, leading to the solidifying of PU and remaining of water inside the fiber.[32,53,54] During the postprocessing of drying, the continuous evaporation of water will generate a porous and uneven surface (Figure 2D). Thanks to the porous structure, the PU fiber has a small density of 0.51 g/cm^3, and the porosity was calculated to be 53.6% according to the equation of $\varphi = (\rho_0 - \rho)/\rho_0 \times 100\%$, where φ, ρ_0, ρ refers to the porosity, PU density, and bulk density of porous fiber, respectively. The high porosity not only reduces the consumption of materials, but also bestows the fiber a much lighter weight, low modulus, as well as high flexibility, which is greatly beneficial to the wearable comfort. After ultrasonication treatment in CB suspension, it can be clearly seen in Figure 2E and Supporting Information: Figure S4A that the porous fiber surface is successfully decorated with abundant CB nanoparticles with a mean particle size of ca. 40 nm. The cross-sectional SEM image of CB@PU in Supporting Information: Figure S4B also reveals that the fiber is wrapped with a continuous and dense CB layer, thus forming conductive pathways on the fiber surface. In addition, after modification by PDA for 3 h, it was reported that a thin PDA film with a thickness of <20 nm will be generated.[47] As shown in Figure 2F, the nanoscale PDA film adheres to the CB layer and binds the neighboring CB nanoparticles closer, resulting in a more compact structure. With improved surface affinity with PDA, the Ag nanoparticles will prefer to deposit on the fiber surface. As depicted in Figure 2G, after Ag plating, the fiber is covered with another type of nanoparticle with a bigger particle size of ca. 235 nm, which is attributed to newly formed Ag nanoparticles as confirmed by the EDS results in Figure 2H. Starting with the PDA-assisted nucleation, these Ag nanoparticles gradually grow, aggregate, and connect closely to each other, finally forming a uniform Ag layer.[55] Furthermore, the colored SEM image on cross-section in Figure 2I (original image was shown in Supporting Information: Figure S5) vividly exhibits the

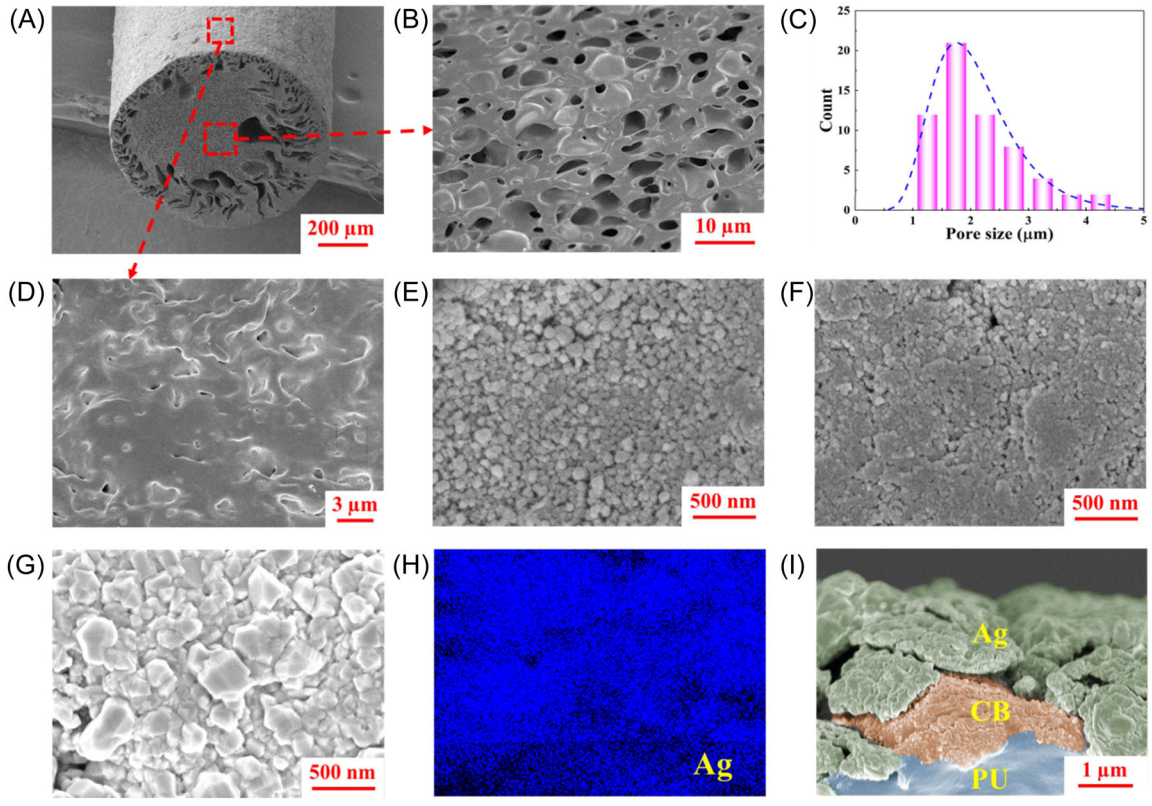

FIGURE 2 Cross-sectional SEM images of (A, B) wet-spun PU fiber. (C) Statistics of the pore diameters in (B). Surficial SEM images of (D) PU, (E) CB@PU, (F) PDA-CB@PU, and (G) Ag/CB@PU fibers, respectively. (H) Ag mapping on the surface of Ag/CB@PU fiber. (I) Cross-sectional SEM image of Ag/CB@PU fiber, showing the multilayered structure. CB, carbon black; PDA, polydopamine; PU, polyurethane; SEM, scanning electron microscope.

26888193x, 2023, 6, Downloaded from https://onlinelibrary.wiley.com/doi/10.1002/smm2.1178 by Hong Kong Poly University, Wiley Online Library on [11/04/2024]. See the Terms and Conditions (https://onlinelibrary.wiley.com/terms-and-conditions) on Wiley Online Library for rules of use; OA articles are governed by the applicable Creative Commons License

three-layer configuration of the Ag/CB@PU composite fiber, with the PU fiber as core substrate (colored by blue), CB as middle layer (colored by orange), and Ag as top layer (colored by green).

As a supplement to morphology observation, XPS is able to reflect the chemical composition on the fiber surface. As displayed in Figure 3A, due to the CB decoration, CB/PU fiber has an obviously increased C1s peak than pure PU fiber. After modification by PDA, there clearly appears the N1s peak in Figure 3B, and meanwhile, the O/C ratio of PDA-CB@PU increased to 0.302 compared with CB@PU (0.206). In consideration of the rich amine and catechol groups in PDA, these results signify the successful formation of PDA layer. As for the Ag/CB@PU fiber, the strong Ag3d and Ag3p peaks can be clearly observed. In addition, the Ag3d spectrum in Figure 3C includes two peaks of $Ag3d_{3/2}$ peak at 374.9 eV and $Ag3d_{5/2}$ at 368.9 eV with a binding energy gap of 6 eV. Since the two characteristic Ag3d peaks are ascribed to the Ag^0 species,[56] the results demonstrate that the Ag layer in Ag/CB@PU is metallic Ag at zero valent state. Moreover, by means of better thermal stability of CB and Ag than PU, TGA can be utilized to quantitatively study the content of CB and Ag deposited on the PU fiber. As shown in Figure 3D, the PU fiber starts to lose weight at about 310 °C and becomes stable at about 550 °C. When

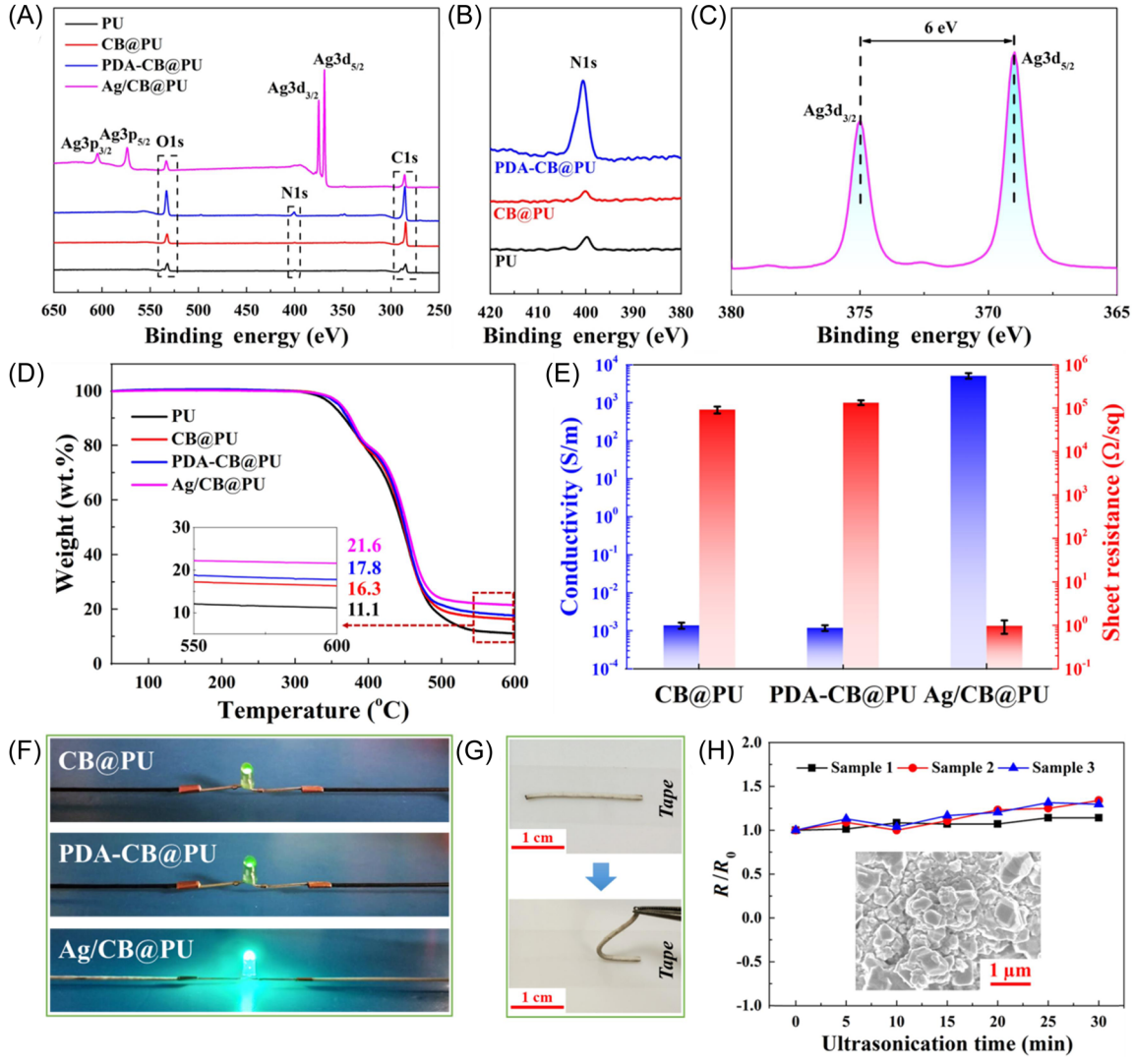

FIGURE 3 (A) XPS spectra of PU fiber and composite fibers with different surface coatings. (B) N1s scans of PU, CB@PU, and PDA-CB@PU fibers. (C) Ag3d scan of Ag/CB@PU fiber. (D) TGA curves of different fibers including pure PU, CB@PU, PDA-CB@PU, and Ag/CB@PU. (E) Conductivity and sheet resistance of CB@PU, PDA-CB@PU, and Ag/CB@PU composite fibers. (F) Lighted LEDs connected by different composite fibers as electrodes and powered by a voltage of 5 V. (G) Photograph showing the peeling test of the Ag/CB@PU fiber. (H) The resistance change's development of three Ag/CB@PU fiber samples under longtime ultrasonication (180 W, 40 kHz). The inset shows SEM morphology after ultrasonication of 30 min. CB, carbon black; LED, light emitting diode; PDA, polydopamine; PU, polyurethane; SEM, scanning electron microscope; TGA, thermogravimetric analysis; XPS, X-ray photoelectron spectroscopy.

26888193x, 2023, 6, Downloaded from https://onlinelibrary.wiley.com/doi/10.1002/smm2.1178 by Hong Kong Poly University, Wiley Online Library on [11/04/2024]. See the Terms and Conditions (https://onlinelibrary.wiley.com/terms-and-conditions) on Wiley Online Library for rules of use; OA articles are governed by the applicable Creative Commons License

heating up to 600 °C, there leaves a residual weight of 11.1 wt% for PU. In contrast, the CB@PU, PDA-CB@PU, and Ag/CB@PU fibers present a higher residual weight of 16.3 wt%, 17.8 wt%, and 21.6 wt%, respectively. Accordingly, the CB percentage in CB@PU can be calculated to be 6.2 wt%,[42,44] while the CB and Ag percentage in Ag/CB@PU is approximately 5.9 wt% and 4.8 wt%. The successive loading of CB and Ag grants the PU fiber good conductivity to transfer electrons on its surface. Figure 3E depicts the conductivity and sheet resistance of the composite fibers with different surface coatings. The conductivity (σ) was obtained by formula of $\sigma = l/SR$, where l, S, and R is the length, cross-sectional area, and volume resistance of fiber, respectively. The CB@PU fiber presents a conductivity of 1.38 mS/m and a sheet resistance of 92.0 kΩ/sq. The PDA modification slightly decreases the conductivity to 1.2 mS/m and increases the sheet resistance to 133.8 kΩ/sq. In clear contrast, with the coating of the top metallic Ag layer, the Ag/CB@PU fiber owns a much higher conductivity of 5139.9 S/m and greatly decreased sheet resistance of 1.0 Ω/sq. This high conductivity of the Ag/CB@PU fiber enables it as highly conductive and flexible electrodes to interconnect different electronics with less power dissipation. As a proof of concept, in Figure 3F the light emitting diode (LED) connected by Ag/CB@PU fibers exhibits vivid brightness, while the LEDs of CB@PU and PDA-CB@PU fibers are very dim. Moreover, it is worth noting that the nano-sized PDA film serves as strong adhesive interface to bond the CB and Ag layers together, which is in favor of a good stability for the composite fiber. As shown in Figure 3G, no shedding of CB and Ag layer can be observed after adhesion test. Additionally, in Figure 3H, the Ag nanoparticles still adhere onto the fiber surface and the fibers' resistance stays stable even after long time (30 min) and high-intensity (180 W and 40 kHz) ultrasonication. The Ag/CB@PU fiber is also stable enough to resist the intense washing process. As displayed in Supporting Information: Figure S6, the fiber appearance presents negligible change after washing, and meanwhile, the SEM images show that the top Ag layer stays almost intact except for some tiny cracks after washing. These both demonstrate the prominent stability of Ag/CB@PU fiber, which is of great significance in practical applications. According to the sensitivity definition of GF for strain sensor, $GF = \Delta R/(R_0 \times \varepsilon)$, where R_0, ΔR, ε represents the initial resistance, resistance change, and applied strain, one can learn that a smaller value of R_0 contributes to a higher GF. Hence, the Ag/CB@PU fiber with high conductivity is expected to exhibit a high sensitivity, and meanwhile, the stable structure assisted by PDA will also grant the fiber sensor a notable stability under cyclic stretching-releasing test.

In addition to electrical conductivity, the dual Ag and CB layers can also deform under strain and generate resistance change because of the modulus mismatch with the soft PU substrate, thus making the Ag/CB@PU fiber a desirable candidate as strain sensor. Before the electromechanical test, the fiber sensor was first trained via a cyclic stretching-releasing process at 200% strain to induce the formation of cracks throughout the conductive layers (Supporting Information: Figure S7). After the strain is released, the cracks will close again to form electrically conductive paths. In fact, the prestretching treatment can reconstruct the conductive network and partly increase the initial resistance, which is believed to improve the repeatability of the sensor.[23,57–59] The electromechanical characteristics of the Ag/CB@PU fiber sensor are depicted in Figure 4A. It can be seen that the electrical resistance increases monotonically with increasing strain, and a relative resistance change of 5.03×10^6 is observed at a large strain of 200%, corresponding to an average GF of 2.52×10^6. In detail, the curve can be approximately divided into five linear regions with increasing GF values as follows: 0%–40% (GF_1 of 2552), 40%–60% (GF_2 of 88696), 60%–120% (GF_3 of 683452), 120%–150% (GF_4 of 3024511), and 150%–200% (GF_5 of 7395386). Furthermore, the CB@PU and Ag@PU composite fibers are tested and compared as shown in Supporting Information: Figure S8. In clear contrast, the CB@PU sensor displays a much smaller relative resistance change of 140 at 200% strain with a GF of 70, while the Ag@PU sensor possess high sensitivity with GF of 309, but low stretchability of ca. 70% at the absence of CB. The contrary sensing characteristics between CB@PU and Ag@PU sensors indicate the completely different strain-responsive mechanisms of CB and Ag layer under strain. By taking advantage of their complementary characteristics, the Ag/CB@PU sensor achieves both high sensitivity and wide working range, clearly verifying the superiority of dual layers over a single Ag or CB layer.

Figure 4B shows the response of the Ag/CB@PU fiber sensor to cyclic stretching-releasing of different strains from 50% to 200%. The stable output curves manifest that the sensor can well detect various strains, making it suitable to monitor different movements of the human body. Moreover, as shown in Figure 4C, it is worth noting that the sensor is also capable of perceiving tiny strains that regular and stable signals can be generated under strains of only 0.3% and 0.1%, further indicating the high sensitivity. In addition to sensitivity and stretchability, the electrical resistance–strain hysteresis during cyclic testing is another important factor for flexible strain sensor. Figure 4D depicts the relative resistance change curves of the sensor under one

26888193x, 2023, 6, Downloaded from https://onlinelibrary.wiley.com/doi/10.1002/smm2.1178 by Hong Kong Poly University, Wiley Online Library on [11/04/2024]. See the Terms and Conditions (https://onlinelibrary.wiley.com/terms-and-conditions) on Wiley Online Library for rules of use; OA articles are governed by the applicable Creative Commons License

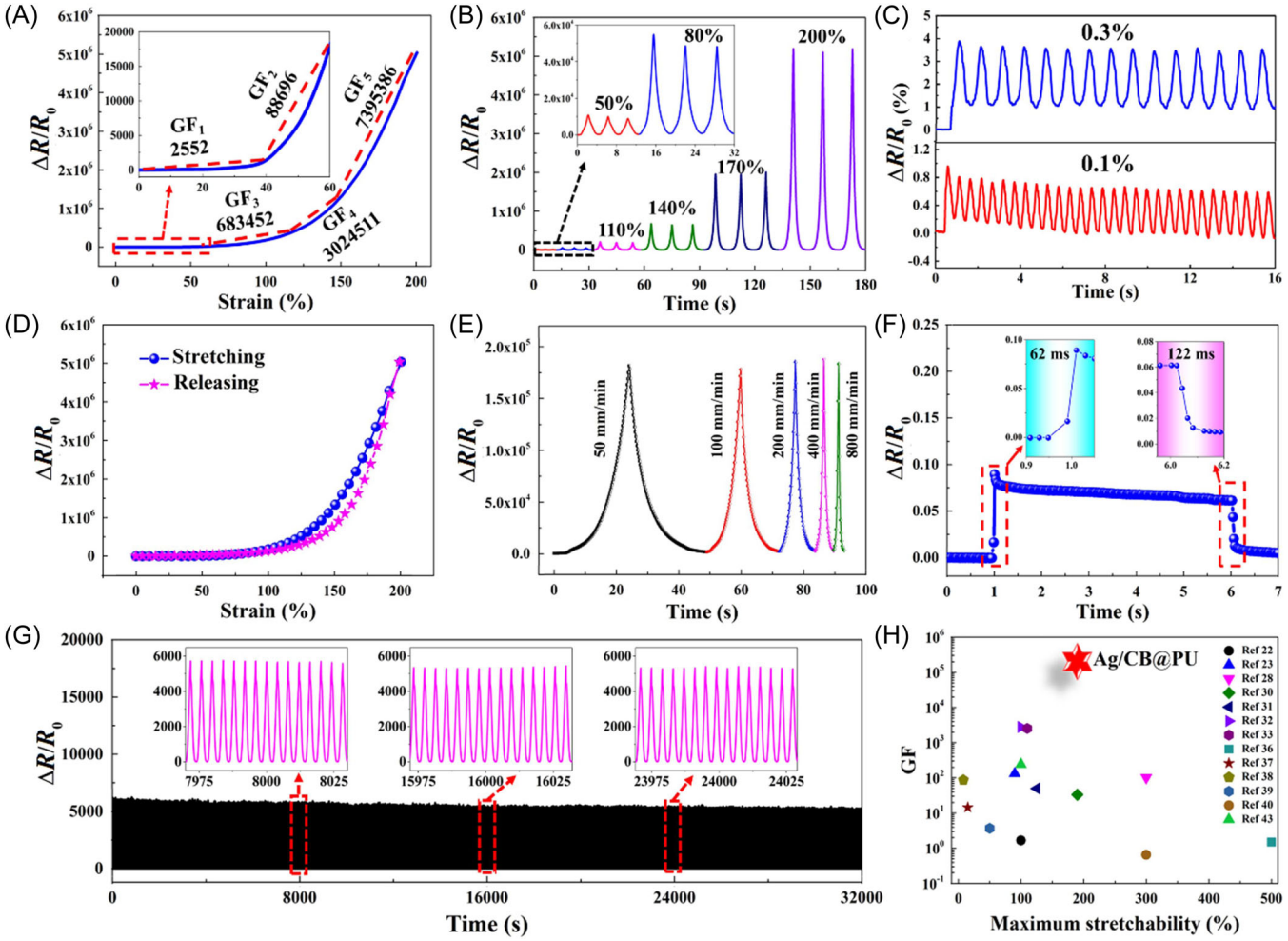

FIGURE 4 (A) Typical relative resistance change-strain curve of Ag/CB@PU fiber sensor at a stretching speed of 300 mm/min. The inset shows the curve within 60% strain. (B) Relative resistance change under various cyclic strains from 50% to 200% at a stretching speed of 300 mm/min. (C) Relative resistance change under tiny strains of 0.1% and 0.3% at a stretching speed of 10 mm/min. (D) Hysteresis behavior of the Ag/CB@PU fiber sensor. (E) Relative resistance response of the sensor to different testing speed at 100% strain. (F) Relative resistance response of the sensor to a small strain of 0.5% under speed of 300 mm/min, showing the response and recovery time. (G) Durability test of the sensor at 50% strain and speed of 300 mm/min for 8000 cycles. (H) Comparison of the GF and maximum working range between Ag/CB@PU sensor in this work and other reported fiber-based strain sensors. CB, carbon black; GF, gauge factor; PU, polyurethane.

stretching-releasing cycle. It can be seen that the resistance can basically return to the initial value along with the strain release, and the hysteresis error can be calculated to be ca. 11.2%.[60,61] The slight hysteresis suggests the good recovery capability of the conductive network. Figure 4E displays the sensor's response to strain with different testing speeds, and the nearly same output signals prove the sensor's fast response and frequency-independent sensing behavior. Meanwhile, in Figure 4F, the response and recovery time of the sensor was tested to be 62 ms and 122 ms. The fast response to external strain is of great importance to monitor human body deformations with varying frequencies. In practical applications, the long-term durability is also considered as an indispensable requirement for the sensor to meet. As shown in Figure 4G, during the multicycle tests at 50% strain, the output curves of the sensor maintain high consistency and repeatability for over 8000 cycles, verifying the excellent cycling stability of the Ag/CB@PU fiber sensor, which can be attributed to the regular deformation and high recovery ability of the Ag/CB conductive network under stretching/releasing cycles. To compare the sensing performance between the Ag/CB@PU and other reported fiber-based strain sensors, Figure 4H plots a map of the maximum values of both GF and workable strain for a series of strain sensors. It is visible that these previous strain sensors usually present low sensitivity and/or narrow workable strain ranges, while the Ag/CB@PU sensor has achieved both a high GF of 2.52×10^6 and a wide working strain of 200% via

26888194x, 2023, 6, Downloaded from https://onlinelibrary.wiley.com/doi/10.1002/smm2.1178 by Hong Kong Poly University, Wiley Online Library on [11/04/2024]. See the Terms and Conditions (https://onlinelibrary.wiley.com/terms-and-conditions) on Wiley Online Library for rules of use; OA articles are governed by the applicable Creative Commons License

the novel design of Ag/CB hybrid architecture, making it a competitive candidate for strain-sensing applications.

The outstanding sensing performance of the Ag/CB@PU sensor is definitely attributed to its conductive bilayer structure, which involves the upper brittle Ag layer of densely stacked Ag nanoparticles and the lower flexible layer of CB-decorated porous PU fiber. The strain sensor can generate electrical signals of resistance change with the loading of external mechanical strains, and the signal of resistance change relies on the deformation of conductive networks and integrity of conductive paths in the dual Ag/CB layers. Hence, to reveal the working mechanism of the Ag/CB@PU strain sensor, the morphology development of the sensor under different strains was tracked by SEM observation. As shown in Figure 5A, there remain abundant tiny cracks on the surficial Ag layer after prestretching. Upon further stretching, the cracks are prone to propagate along the original cracks. When stretched to 100% strain in Figure 5B, the top Ag layer forms a typical island-crack network structure, and the gradually expanded cracks greatly hinder the conductive pathways, thus leading to the rapid increment of electrical resistance as well as the high sensitivity. In particular, the strongly adhesive PDA interface between Ag and CB layers is believed to facilitate the formation of network cracks, because the PDA-reinforced interface can restrict the strain localization and possible delamination of the Ag layer,[62] and finally the deformation of Ag layer is uniform along the strain direction. Besides the cracks in the Ag layer, the CB layer also plays an important role in excellent sensing performance. As shown in Figure 5E, the neighboring Ag islands across the cracks are bridged by the below CB layer, and from the zoom-in view in Figure 5D, the CB nanoparticles connect with each other to provide certain electrical conductance. Additionally, it is worth noting that the pores on the CB layer come from the porous PU substrate instead of cracks generated during stretching. Because there originally exist a great deal of pores on the CB@PU fiber under 0% strain (Supporting Information: Figure S4A), and it is clear in Supporting Information: Figure S9 that the pores of CB@PU fiber are squeezed along the stretching direction under strain, while the propagation of cracks is perpendicular to the stretching direction. On the other hand, it is generally considered that the strain-responsive mechanism of CB@PU composite lies in the tunneling effect.[43,44] As shown in Supporting Information: Figure S10, the relative resistance change versus strain curve of CB@PU sensor can be well fitted with the tunneling model, further proving that tunneling effect dominates the strain-responsive behavior of CB@PU sensor. Therefore, no destructive cracks will be produced for CB@PU sensor under strain, which benefits the integrity of the conductive pathway under large strain. As further evidence, Figure 5C displays the morphology of Ag and CB layers under a larger strain of 150%. It can be seen that the crack proportion of Ag layer is greatly increased and the neighboring Ag islands are almost disconnected from each other, but the underlying CB layer in Figure 5F can still accommodate the high strain by simultaneous deformation with the elastic PU fiber, thus granting the sensor a wide working range.

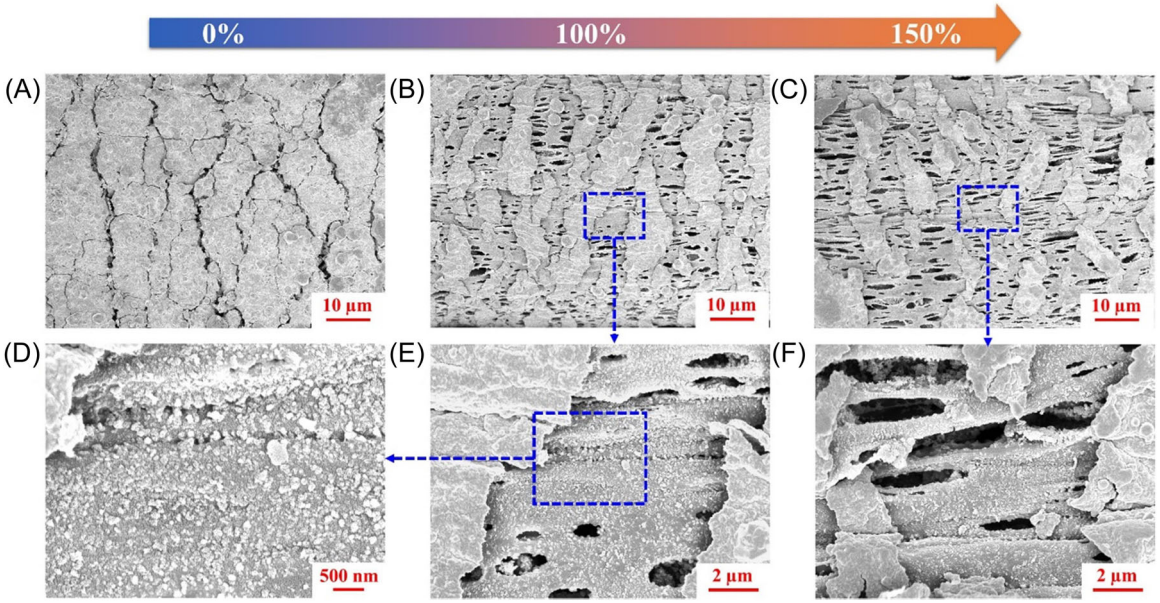

FIGURE 5 SEM images showing the morphologies' development of Ag/CB@PU strain sensor under increasing strains of (A) 0%, (B, D, E) 100%, and (C, F) 150%. CB, carbon black; PU, polyurethane; SEM, scanning electron microscope.

2688819x, 2023, 6, Downloaded from https://onlinelibrary.wiley.com/doi/10.1002/smm2.1178 by Hong Kong Poly University, Wiley Online Library on [11/04/2024]. See the Terms and Conditions (https://onlinelibrary.wiley.com/terms-and-conditions) on Wiley Online Library for rules of use; OA articles are governed by the applicable Creative Commons License

The scheme in Figure 6A is proposed to illustrate the sensing mechanism of Ag/CB@PU strain sensor. Upon stretching, the brittle Ag layer is gradually destructed into an island-crack structure, and the Ag islands will become entirely isolated with the increasing propagation of cracks at high strain level. Certainly, such continuous and drastic interruption of conductive pathways will contribute to a high sensitivity during the whole stretching process. Meanwhile, with the aid of the tunneling effect, the CB layer is more flexible to bear much larger strain, which makes it capable of serving as a bridge to connect adjacent Ag islands, thus ensuring the sensor a wide working range. According to the applied strain level, there are two routes to effectively transfer electrons across the conductive network, which can also be simply described by the resistance model in Figure 6B. Under small strains, the cracks are narrow and the neighboring Ag islands are still able to connect with each other. In this case, electrons prefer to transfer along the Ag layer because of its much higher conductivity than CB layer, and the total resistance can be calculated by the following equation:[63,64]

$$R = \frac{2R_{Ag_1}R_{Ag_2} + 2R_{Ag_1}R_{CB} + R_{Ag_2}R_{CB}}{R_{Ag_2} + R_{CB}}, \quad (1)$$

where R_{Ag_1}, R_{Ag_2}, and R_{CB} refers to the resistance of Ag islands, Ag bridge between two neighboring Ag islands, and CB layer below the Ag cracks, respectively. During earlier stretching, the value of R_{Ag_1} can be basically assumed as constant. The increasing R_{Ag_2} from the crack propagation contributes to the most increment of total resistance, and the effect of R_{CB} will become more and more obvious as its value approaches to that of rapidly increasing R_{Ag_2}. As the strain further increases to a higher level, the crack gap grows wider, finally giving rise to the complete disconnection of adjacent Ag islands, and then the lower CB layer will take charge of electron transportation to make sure the adjacent Ag islands are electrically connected. In this regard, the value of R_{Ag_2} is considered as infinite, and the equation can be approximated as $R = 2R_{Ag_1} + R_{CB}$, indicating that the resistance increment under high strain comes from the future rupturing of Ag islands and increasing tunneling resistance of CB layer. Overall, the synergistic effect of crack-based Ag layer and tunneling effect-based CB layer endows the sensor both high sensitivity and wide working range.

For the purpose of comfortable wearability, the as-prepared Ag/CB@PU fiber sensor was integrated into a specially designed fabric structure by weaving. The supporting fabric adopts a modified Bedford cord structure featuring longer yarn floats and less binding points between the warp and weft yarns. As schemed in Figure 7A, in this structure the fiber sensor is in a straight configuration along the strain direction, and meanwhile with few bindings with other yarns, which can reduce internal friction between the sensor and other yarns, thus improving the hysteresis and repeatability of the sensor. Additionally, the spandex/cotton core-spun yarn, with high stretchability and elastic recovery, was chosen as the weft yarn, in which the spandex core offers the superior elasticity, and the cotton contributes to an extended service life and soft hand feeling. Besides, it is noteworthy that the stretchability of this core-spun yarn is comparable with that of the PU fiber-based sensor, so

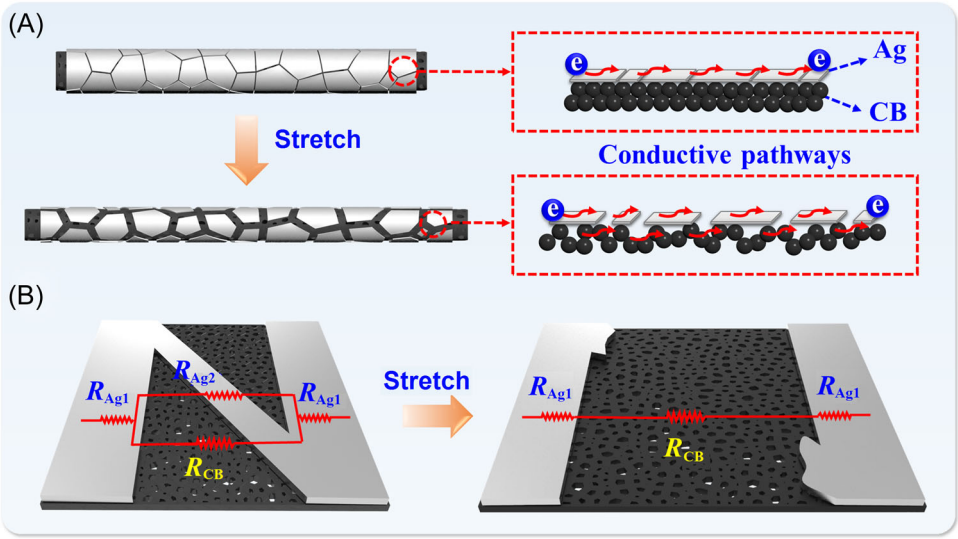

FIGURE 6 (A) Scheme illustrating the sensing mechanism of Ag/CB@PU sensor during stretching. (B) Resistance model of the sensor under different strains. CB, carbon black; PU, polyurethane.

26888194x, 2023, 6, Downloaded from https://onlinelibrary.wiley.com/doi/10.1002/smm2.1178 by Hong Kong Poly University, Wiley Online Library on [11/04/2024]. See the Terms and Conditions (https://onlinelibrary.wiley.com/terms-and-conditions) on Wiley Online Library for rules of use; OA articles are governed by the applicable Creative Commons License

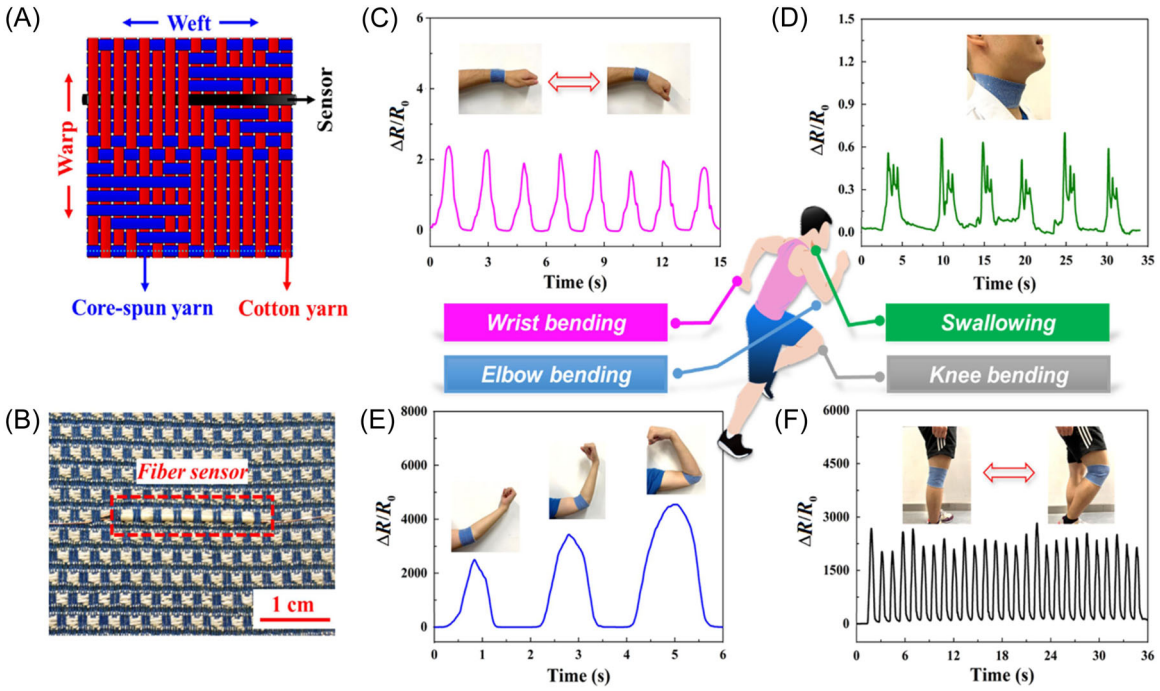

FIGURE 7 Wearable demonstrations of the sensing fabric integrated with the Ag/CB@PU fiber sensor: (A) architecture and (B) photograph of the designed sensing fabric with a modified Bedford cord structure. The photos and corresponding signals of the sensors for different human motion detection including (C) wrist bending, (D) swallowing, (E) elbow bending, and (F) knee bending. CB, carbon black; PU, polyurethane.

that the Ag/CB@PU fiber sensor can deform in step with the supporting fabric in the weft direction. Cotton yarn was applied as the warp yarn because of its good wearability and wide application. Along the weft direction, the fiber sensor was inserted in a certain position with less binding points between the weft and warp yarns, which is beneficial to reduce the friction between the fiber sensor and supporting fabric. Figure 7B shows the photograph of the obtained sensing fabric. One can see that the small-sized and lightweight fiber sensor is seamlessly integrated within the fabric structure, presenting negligible influence on the fabric's appearance and air permeability. Featuring of good wearability, the sensing fabric can provide friendly contact with human skin for readily monitoring various human motions. As displayed in Figure 7C, the sensing fabric was conformally fixed around the wrist as a smart band, and regular signals could be well collected during the periodical wrist bending. In addition, the high sensitivity also enables the Ag/CB@PU sensor to detect some subtle motions. For example, in Figure 7D, by mounting the sensor onto a volunteer's neck, the complex throat movements during swallowing were accurately captured with a high repeatability. Figure 7E presents the sensor's application in monitoring large human motions of elbow bending. When the elbow was gradually bent to a larger degree, the sensor can generate varying signals with elevated relative resistance change, suggesting the high sensing accuracy. Furthermore, the sensor is also competent to work under high frequency. As a proof in Figure 7F, the fast knee bending during walking can be clearly recognized, and it is also of great importance that the notable wearability of the sensing fabric well assures the wearing comfort during long-term testing. All of the above experiments demonstrate that our Ag/CB@PU strain sensor can be applied to monitor a variety of human motions, showing huge potential in diverse applications of health monitoring, sports motion tracking, intelligent robotics and so on.

4 | CONCLUSIONS

In summary, we have prepared a highly stretchable and conductive fiber strain sensor of Ag/CB@PU, which contains a core porous PU fiber, and an outer sheath of dual Ag/CB nanoparticles conductive layers. The strain-responsive behavior of the sensor was systematically studied, and the results of morphology development reveal the crack propagation-based mechanism of brittle Ag layer and tunneling effect-based mechanism of flexible CB@PU layer. Benefiting from the synergetic effect of Ag/CB conductive configuration, the Ag/CB@PU strain sensor presents outstanding sensing

26888193x, 2023, 6, Downloaded from https://onlinelibrary.wiley.com/doi/10.1002/smm2.1178 by Hong Kong Poly University, Wiley Online Library on [11/04/2024]. See the Terms and Conditions (https://onlinelibrary.wiley.com/terms-and-conditions) on Wiley Online Library for rules of use; OA articles are governed by the applicable Creative Commons License

performance, including ultrahigh sensitivity with a GF of up to 2.52×10^6, wide working range of 200%, low detection limit of 0.1%, fast response time of 62 ms and a recovery time of 122 ms, and notable stability of 8000 cycles. Moreover, this lightweight fiber sensor can be readily integrated into a fabric structure. Combining the sensing function of Ag/CB@PU fiber and good wearability of fabric, the obtained sensing fabric well demonstrate applications for real-time monitoring various human motions. This work proposed a new strategy for the facile preparation of conductive composite fibers by combining wet-spinning technology and hybrid conductive configuration, promising the stretchable and wearable sensing for human-centered applications.

ACKNOWLEDGMENTS

This study was supported by the Research Grant Council of Hong Kong (No. 15209420).

CONFLICTS OF INTEREST STATEMENT

The authors declare no conflicts of interest.

DATA AVAILABILITY STATEMENT

The data that support the findings of this study are available in the supplementary material of this article.

ORCID

Tao Hua https://orcid.org/0000-0001-9596-5830

REFERENCES

1. Amjadi M, Kyung KU, Park I, Sitti M. Stretchable, skin-mountable, and wearable strain sensors and their potential applications: a review. *Adv Funct Mater*. 2016;26(11):1678-1698.
2. Gao Y, Yu L, Yeo JC, Lim CT. Flexible hybrid sensors for health monitoring: materials and mechanisms to render wearability. *Adv Mater*. 2020;32(15):1902133.
3. Zhou K, Dai K, Liu C, Shen C. Flexible conductive polymer composites for smart wearable strain sensors. *SmartMat*. 2020;1(1):e1010.
4. Gao J, Fan Y, Zhang Q, et al. Ultra-robust and extensible fibrous mechanical sensors for wearable smart healthcare. *Adv Mater*. 2022;34(20):2107511.
5. Yin R, Wang D, Zhao S, Lou Z, Shen G. Wearable sensors-enabled human-machine interaction systems: from design to application. *Adv Funct Mater*. 2021;31(11):2008936.
6. Yin Z, Lu H, Gan L, Zhang Y. Electronic fibers/textiles for health-monitoring: fabrication and application. *Adv Mater Technol*. 2023;8:2200654.
7. Zhang Y, Lu H, Liang X, et al. Silk materials for intelligent fibers and textiles: potential, progress and future perspective. *Acta Phys-Chim Sin*. 2022;38(9):2103034.
8. Gan L, Zeng Z, Lu H, et al. A large-scalable spraying-spinning process for multifunctional electronic yarns. *SmartMat*. 2023;4(2):e1151.
9. Liu X, Miao J, Fan Q, et al. Recent progress on smart fiber and textile based wearable strain sensors: materials, fabrications and applications. *Adv Fiber Mater*. 2022;4(571):361-389.
10. Seyedin S, Zhang P, Naebe M, et al. Textile strain sensors: a review of the fabrication technologies, performance evaluation and applications. *Mater Horiz*. 2019;6(2):219-249.
11. Wang J, Lu C, Zhang K. Textile-based strain sensor for human motion detection. *Energy Environ Mater*. 2020;3(1):80-100.
12. Bi S, Hou L, Zhao H, Zhu L, Lu Y. Ultrasensitive and highly repeatable pen ink decorated cuprammonium rayon (cupra) fabrics for multifunctional sensors. *J Mater Chem A*. 2018;6(34):16556-16565.
13. Cai G, Yang M, Xu Z, Liu J, Tang B, Wang X. Flexible and wearable strain sensing fabrics. *Chem Eng J*. 2017;325:396-403.
14. Luo J, Gao S, Luo H, et al. Superhydrophobic and breathable smart MXene-based textile for multifunctional wearable sensing electronics. *Chem Eng J*. 2021;406:126898.
15. Ren J, Wang C, Zhang X, et al. Environmentally-friendly conductive cotton fabric as flexible strain sensor based on hot press reduced graphene oxide. *Carbon*. 2017;111:622-630.
16. Lee T, Lee W, Kim SW, Kim JJ, Kim BS. Flexible textile strain wireless sensor functionalized with hybrid carbon nanomaterials supported ZnO nanowires with controlled aspect ratio. *Adv Funct Mater*. 2016;26(34):6206-6214.
17. Yang Z, Pang Y, Han X, et al. Graphene textile strain sensor with negative resistance variation for human motion detection. *ACS Nano*. 2018;12(9):9134-9141.
18. Lu D, Liao S, Wei Q, Xiao X, Wang Q. Comparative study of different carbon materials for the preparation of knitted fabric sensors. *Cellulose*. 2022;29(13):7431-7444.
19. Liu Z, Zhu T, Wang J, et al. Functionalized fiber-based strain sensors: pathway to next-generation wearable electronics. *Nano-Micro Lett*. 2022;14(1):61.
20. Lee J, Zambrano BL, Woo J, Yoon K, Lee T. Recent advances in 1D stretchable electrodes and devices for textile and wearable electronics: materials, fabrications, and applications. *Adv Mater*. 2020;32(5):1902532.
21. Seyedin S, Moradi S, Singh C, Razal JM. Continuous production of stretchable conductive multifilaments in kilometer scale enables facile knitting of wearable strain sensing textiles. *Appl Mater Today*. 2018;11:255-263.
22. Li Y, Zhou B, Zheng G, et al. Continuously prepared highly conductive and stretchable SWNT/MWNT synergistically composited electrospun thermoplastic polyurethane yarns for wearable sensing. *J Mater Chem C*. 2018;6(9):2258-2269.
23. Niu B, Hua T, Hu H, et al. A highly durable textile-based sensor as a human-worn material interface for long-term multiple mechanical deformation sensing. *J Mater Chem C*. 2019;7(46):14651-14663.
24. Shang Y, Li Y, He X, et al. Highly twisted double-helix carbon nanotube yarns. *ACS Nano*. 2013;7(2):1446-1453.
25. Wang X, Qiu Y, Cao W, Hu P. Highly stretchable and conductive core-sheath chemical vapor deposition graphene fibers and their applications in safe strain sensors. *Chem Mater*. 2015;27(20):6969-6975.
26. Peng S, Yu Y, Wu S, Wang C-H. Conductive polymer nanocomposites for stretchable electronics: material selection, design, and applications. *ACS Appl Mater Interfaces*. 2021;13(37):43831-43854.

26888194x, 2023, 6, Downloaded from https://onlinelibrary.wiley.com/doi/10.1002/smm2.1178 by Hong Kong Poly University, Wiley Online Library on [11/04/2024]. See the Terms and Conditions (https://onlinelibrary.wiley.com/terms-and-conditions) on Wiley Online Library for rules of use; OA articles are governed by the applicable Creative Commons License

27. Liu H, Li Q, Zhang S, et al. Electrically conductive polymer composites for smart flexible strain sensors: a critical review. *J Mater Chem C*. 2018;6(45):12121-12141.
28. Yu Y, Zhai Y, Yun Z, et al. Ultra-stretchable porous fiber-shaped strain sensor with exponential response in full sensing range and excellent anti-interference ability toward buckling, torsion, temperature, and humidity. *Adv Electron Mater*. 2019;5(10):1900538.
29. Han S, Liu C, Xu H, et al. Multiscale nanowire-microfluidic hybrid strain sensors with high sensitivity and stretchability. *npj Flex Electron*. 2018;2(1):16.
30. Li Z, Qi X, Xu L, et al. Self-repairing, large linear working range shape memory carbon nanotubes/ethylene vinyl acetate fiber strain sensor for human movement monitoring. *ACS Appl Mater Interfaces*. 2020;12(37): 42179-42192.
31. Montazerian H, Rashidi A, Dalili A, Najjaran H, Milani AS, Hoorfar M. Graphene-coated spandex sensors embedded into silicone sheath for composites health monitoring and wearable applications. *Small*. 2019;15(17):1804991.
32. He Z, Zhou G, Byun J-H, et al. Highly stretchable multi-walled carbon nanotube/thermoplastic polyurethane composite fibers for ultrasensitive, wearable strain sensors. *Nanoscale*. 2019;11(13): 5884-5890.
33. Wang X, Meng S, Tebyetekerwa M, et al. Highly sensitive and stretchable piezoresistive strain sensor based on conductive poly (styrene-butadiene-styrene)/few layer graphene composite fiber. *Compos, Part A*. 2018;105:291-299.
34. Wang H, Li R, Cao Y, et al. Liquid metal fibers. *Adv Fiber Mater*. 2022;4(5):987-1004.
35. Wu Y, Zhen R, Liu H, et al. Liquid metal fiber composed of a tubular channel as a high-performance strain sensor. *J Mater Chem C*. 2017;5(47):12483-12491.
36. Chen G, Wang H, Guo R, Duan M, Zhang Y, Liu J. Superelastic EGaIn composite fibers sustaining 500% tensile strain with superior electrical conductivity for wearable electronics. *ACS Appl Mater Interfaces*. 2020;12(5):6112-6118.
37. Zhang M, Wang C, Wang Q, Jian M, Zhang Y. Sheath–core graphite/silk fiber made by dry-meyer-rod-coating for wearable strain sensors. *ACS Appl Mater Interfaces*. 2016;8(32): 20894-20899.
38. Huang T, He P, Wang R, et al. Porous fibers composed of polymer nanoball decorated graphene for wearable and highly sensitive strain sensors. *Adv Funct Mater*. 2019; 29(45):1903732.
39. Cheng Y, Wang R, Sun J, Gao L. A stretchable and highly sensitive graphene-based fiber for sensing tensile strain, bending, and torsion. *Adv Mater*. 2015;27(45):7365-7371.
40. Wang Z, Huang Y, Sun J, et al. Polyurethane/cotton/carbon nanotubes core-spun yarn as high reliability stretchable strain sensor for human motion detection. *ACS Appl Mater Interfaces*. 2016;8(37):24837-24843.
41. Niu B, Hua T, Xu B. Robust deposition of silver nanoparticles on paper assisted by polydopamine for green and flexible electrodes. *ACS Sustain Chem Eng*. 2020;8(34):12842-12851.
42. Gao J, Hu M, Dong Y, Li RKY. Graphite-nanoplatelet-decorated polymer nanofiber with improved thermal, electrical, and mechanical properties. *ACS Appl Mater Interfaces*. 2013;5(16):7758-7764.
43. Chen Y, Wang L, Wu Z, et al. Super-hydrophobic, durable and cost-effective carbon black/rubber composites for high performance strain sensors. *Compos Part B Eng*. 2019;176: 107358.
44. Wang X, Liu X, Schubert DW. Highly sensitive ultrathin flexible thermoplastic polyurethane/carbon black fibrous film strain sensor with adjustable scaffold networks. *Nano-Micro Lett*. 2021;13(1):64.
45. Chen J, Yu Q, Cui X, et al. An overview of stretchable strain sensors from conductive polymer nanocomposites. *J Mater Chem C*. 2019;7(38):11710-11730.
46. Wang C, Xia K, Wang H, Liang X, Yin Z, Zhang Y. Advanced carbon for flexible and wearable electronics. *Adv Mater*. 2019;31(9):1801072.
47. Lee H, Dellatore SM, Miller WM, Messersmith PB. Mussel-inspired surface chemistry for multifunctional coatings. *Science*. 2007;318(5849):426-430.
48. Liu Y, Ai K, Lu L. Polydopamine and its derivative materials: synthesis and promising applications in energy, environmental, and biomedical fields. *Chem Rev*. 2014;114(9):5057-5115.
49. Zhu C, Guan X, Wang X, Li Y, Chalmers E, Liu X. Mussel-inspired flexible, durable, and conductive fibers manufacturing for finger-monitoring sensors. *Adv Mater Interfaces*. 2019;6(1):1801547.
50. Wang W, Li R, Tian M, et al. Surface silverized meta-aramid fibers prepared by bio-inspired poly(dopamine) functionalization. *ACS Appl Mater Interfaces*. 2013;5(6):2062-2069.
51. Li X, Hu H, Hua T, Xu B, Jiang S. Wearable strain sensing textile based on one-dimensional stretchable and weavable yarn sensors. *Nano Res*. 2018;11(11):5799-5811.
52. Jur JS, Sweet III WJ, Oldham CJ, Parsons GN. Atomic layer deposition of conductive coatings on cotton, paper, and synthetic fibers: conductivity analysis and functional chemical sensing using "all-fiber" capacitors. *Adv Funct Mater*. 2011;21(11):1993-2002.
53. Yu Y, Zheng G, Dai K, et al. Hollow-porous fibers for intrinsically thermally insulating textiles and wearable electronics with ultrahigh working sensitivity. *Mater Horiz*. 2021;8(3):1037-1046.
54. Wang X, Sun H, Yue X, et al. A highly stretchable carbon nanotubes/thermoplastic polyurethane fiber-shaped strain sensor with porous structure for human motion monitoring. *Compos Sci Technol*. 2018;168:126-132.
55. Yin Y, Li Z-Y, Zhong Z, Gates B, Xia Y, Venkateswaran S. Synthesis and characterization of stable aqueous dispersions of silver nanoparticles through the Tollens process. *J Mater Chem*. 2002;12(3):522-527.
56. Cong Y, Xia T, Zou M, et al. Mussel-inspired polydopamine coating as a versatile platform for synthesizing polystyrene/Ag nanocomposite particles with enhanced antibacterial activities. *J Mater Chem B*. 2014;2(22):3450-3461.
57. Wang C, Xia K, Zhang M, Jian M, Zhang Y. An all-silk-derived dual-mode e-skin for simultaneous temperature-pressure detection. *ACS Appl Mater Interfaces*. 2017;9(45): 39484-39492.

26888194, 2023, 6, Downloaded from https://onlinelibrary.wiley.com/doi/10.1002/smm2.1178 by Hong Kong Poly University, Wiley Online Library on [11/04/2024]. See the Terms and Conditions (https://onlinelibrary.wiley.com/terms-and-conditions) on Wiley Online Library for rules of use; OA articles are governed by the applicable Creative Commons License

58. Zhao S, Guo L, Li J, et al. Binary synergistic sensitivity strengthening of bioinspired hierarchical architectures based on fragmentized reduced graphene oxide sponge and silver nanoparticles for strain sensors and beyond. *Small*. 2017; 13(28):1700944.
59. Lee J, Shin S, Lee S, et al. Highly sensitive multifilament fiber strain sensors with ultrabroad sensing range for textile electronics. *ACS Nano*. 2018;12(5):4259-4268.
60. Li X, Hua T, Xu B. Electromechanical properties of a yarn strain sensor with graphene-sheath/polyurethane-core. *Carbon*. 2017; 118:686-698.
61. Chhetry A, Sharifuzzaman M, Yoon H, Sharma S, Xuan X, Park JY. MoS_2-decorated laser-induced graphene for a highly sensitive, hysteresis-free, and reliable piezoresistive strain sensor. *ACS Appl Mater Interfaces*. 2019;11(25):22531-22542.
62. Zhang C, Sun J, Lu Y, Liu J. Nanocrack-based strain sensors. *J Mater Chem C*. 2021;9(3):754-772.
63. Wang C, Li X, Gao E, et al. Carbonized silk fabric for ultrastretchable, highly sensitive, and wearable strain sensors. *Adv Mater*. 2016;28(31):6640-6648.
64. Wang W, Ma Y, Wang T, et al. Double-layered conductive network design of flexible strain sensors for high sensitivity and wide working range. *ACS Appl Mater Interfaces*. 2022;14(32):36611-36621.

SUPPORTING INFORMATION

Additional supporting information can be found online in the Supporting Information section at the end of this article.

How to cite this article: Niu B, Yang S, Yang Y, Hua T. Highly conductive fiber with design of dual conductive Ag/CB layers for ultrasensitive and wide-range strain sensing. *SmartMat*. 2023;4:e1178. doi:10.1002/smm2.1178

26888319x, 2023, 6, Downloaded from https://onlinelibrary.wiley.com/doi/10.1002/smm2.1178 by Hong Kong Poly University, Wiley Online Library on [11/04/2024]. See the Terms and Conditions (https://onlinelibrary.wiley.com/terms-and-conditions) on Wiley Online Library for rules of use; OA articles are governed by the applicable Creative Commons License